Transition Metal Germylene Complexes in Zeolite Cages: Anchoring and Stability

Aticha Borvornwattananont,† Karin Moller, and Thomas Bein*

Department of Chemistry, Purdue University, West Lafayette, Indiana 47907 *(Received: December 9, 1991; In Final Form: March 13, 1992)*

The surface chemistry of the two germylene complexes $Cl_2(THF)GeM(CO)_5$ (M = Mo (**1**) and W (**2**)) in zeolite Y was studied with X-ray absorption spectroscopy (Ge, Mo, W edge EXAFS) and in situ FTIR/TPD-MS techniques. The molybdenum complex **1** interacts with the framework of Na-Y zeolite at room temperature where decarbonylation occurs to a small extent. The intrazeolite **1** retains the Ge-Mo bond up to about 120 °C. In proton-loaded H-Y zeolite, framework interactions increase with temperature, and the Ge-Mo bond is retained up to about the same temperature. At higher temperatures, the Ge-Mo bond is cleaved and $MoCl_x$ and Mo-Mo species are formed in the Na-Y and H-Y forms, respectively. $GeCl_x$ fragments attach to both zeolite frameworks. The intrazeolite complex $Cl_2(THF)GeW(CO)_5$ (**2**) retains all five carbonyl ligands up to about 100 °C in both Na-Y and the proton form. Significant anchoring through the Ge moiety is observed at room temperature in Na-Y and at about 80 °C in the proton form. The intrazeolite stability of the anchored Ge-W complex is somewhat higher than that of the Ge-Mo analog, and WCl_x species are formed upon cleavage of the Ge-W bond at higher temperatures. The anchoring of the $Cl_2(THF)Ge$ moiety into Na-Y is believed to be based upon a Na^+--Cl^- interaction between Na ions in zeolite coordination sites and the chloride ligands of the precursor. The only gas evolution detected up to about 120 °C is due to partial decarbonylation (CO) and HCl formation in the acid supports. The absence of precursor desorption confirms the effective anchoring of the transition-metal germylene complexes into zeolite cages.

Introduction

Immobilization strategies of transition-metal catalysts on heterogeneous supports have attracted increasing attention:[1-3] The advantages of many molecular catalysts,[4] such as high selectivity, mild reaction conditions, and utilization of all metal atoms, could potentially be combined with the facile product separation and catalyst recovery inherent in heterogeneous systems. Combined "hybrid" systems could also offer features not present in conventional catalysts: The immobilized, catalytically active centers might be stabilized against aggregation, and they could be used in reaction media in which the original molecular catalyst is insoluble, or even in gas-solid interface reactions. However, hybrid systems can also present complications, including the frequent instability against leaching of the catalyst metal into solution and agglomeration resulting in (undesired) metal particles with different catalytic reactivity.

This article describes a comprehensive study of the chemistry of Ge-metal complexes in zeolite cages. As part of our efforts to develop novel immobilization concepts for organometallic fragments in porous solids, we have introduced heterobinuclear compounds as candidates for linking catalytic functions to zeolite frameworks. The premise is that the complexes can be anchored to the support via an oxophilic element, whereas catalytic reactions may proceed at the second metal center. This anchoring concept is aimed at the stabilization of the metal species against agglomeration under reducing conditions. Complexes such as $Cl_2(THF)GeMo(CO)_5$, described below, can diffuse into zeolite Y cages because their cross section is similar to that of $Mo(CO)_6$, a molecule frequently studied in this zeolite host.[3]

Zeolites are crystalline, open framework oxide structures (classically aluminosilicates) with pore sizes between 0.3 and 1.2 nm and exchangeable cations compensating for the negative charge of the framework.[5,6] The present work focuses on the use of zeolite Y with 1.2-nm large supercages (SC) connected by 0.75-nm windows. Alkali metal cations coordinated to oxygen-metal rings (with C_{3v} and C_{2v} symmetry in zeolite Y) can be exchanged with NH_4^+ to obtain the acid form by degassing at elevated temperatures.[7]

$$NH_4OZ \rightarrow NH_3 + HOZ$$

OZ, zeolite framework oxygen ions

Reactant, product or transition-state shape selectivity[8] can offer a wide control of *selectivity* that is conceptually unique to the well-defined molecular sieves. A number of previous studies have been aimed at the deposition of catalytically active organometallics into zeolites. Neutral metal carbonyls have been adsorbed in large-pore zeolites, primarily in faujasite-type structures.[9,10] We have recently shown that zeolite metal cations such as Na^+ provide weak binding sites for the carbonyl ligands.[11] However, this interaction does not prevent carbonyl complexes such as $Ni(CO)_4$,[12] $Fe(CO)_5$, or $Mo(CO)_6$ from diffusion, migration out of the pore system, and eventual agglomeration at elevated temperatures.[13,14]

Transition-metal cations can be introduced into the zeolite framework via ion exchange and subsequent exposure to ligands to form complexes. Intrazeolite Ru,[15] Ir,[16] and particularly Rh carbonyl complex cations have been studied in great detail,[17-19] but agglomeration is a frequent problem with these systems. Intrazeolite Co^{II}salen has been prepared by Co(II) ion exchange and successive reaction with the ligand.[20] Similarly, Fe-phthalocyanine[21] complexes were synthesized in zeolite cavities. In analogy to the surface chemistry of transition-metal allyl complexes on amorphous oxide supports,[22-24] the reaction of $Rh(allyl)_3$ with partially proton-exchanged X- and Y-type zeolites has been reported.[25-28] The formation of intrazeolite Rh-CO and Rh-hydride species as inferred from infrared data indicated that the anchored Rh-allyl fragments reacted similar to the complex in solution.

A preliminary report on our intrazeolite attachment of $Cl_2(THF)GeMo(CO)_5$ has been published.[29] The present article describes a detailed analysis of the chemistry of this complex and its tungsten analog in different forms of zeolites Y. The study addresses the anchoring process and the stability of the complexes as a function of zeolite acidity, the nature of the transition metal, and temperature.

Experimental Section

Sample Preparation. Precursors $Cl_2(THF)GeMo(CO)_5$ (**1**) (mp 96-98 °C) and $Cl_2(THF)GeW(CO)_5$ (**2**) (mp 104-106 °C) were synthesized following a method reported for complex **2** using a Schlenk apparatus with Teflon valves.[30] The complexes were characterized by IR, ^1H and ^{13}C NMR, EXAFS, and mass spectrometries. NMR measurements were carried out using a Bruker 250 spectrometer. Mass spectra were taken with a Finnigan mass spectrometer by heating the complexes from 50 to 200 °C at a rate of 20 °C/min. The $M(CO)_5$ moiety of the precursors can be considered to have C_{4v} symmetry which should have three IR bands in the CO stretching region (2 A_1 + 1 E). The position of the carbonyl bands of **1** and **2** depends strongly on solvents; however, two major CO bands at 2083 (A_1) and 1958 cm^{-1} (E)

* To whom correspondence should be addressed.
† Present address: Department of Chemistry, Chulalongkorn University, Bangkok 10330, Thailand.

0022-3654/92/2096-6713$03.00/0 © 1992 American Chemical Society

in CH_2Cl_2 for **1** and 2080 and 1948 cm^{-1} for **2** are comparable to other $LM(CO)_5$ complexes.[31] The other A_1 mode is missing due to very weak absorption as often found for these structures.[32] The ^1H NMR data show two characteristic peaks of coordinated THF at 2.22 and 4.43 ppm for **1** and 2.21 and 4.43 ppm for **2**, respectively. Both appear at lower field compared to free THF (1.51 and 3.39 ppm) in the same solvent. The ^{13}C NMR resonances of the carbonyl ligands of 4:1 intensity ratio at 204 and 209 ppm for **1** and 195 and 198 ppm for **2** are comparable to those of other $LM(CO)_5$ compounds.[33] The mass spectrum of **1** shows dominant peaks due to THF (mass 72) and CO (mass 28) as well as a trace of **1**–THF (mass 379.6) and **1**–THF–*n*CO peaks. No molecular peaks for **1** (at 451.6) or **2** (at 539.5) were detected using 30-eV ionization energy.

Intrazeolite Absorption. The above precursors **1** and **2** were absorbed into two different supports: Na–Y (commercial Linde LZ-Y52 $[Na_{57}Al_{57}Si_{135}O_{384}]\cdot 235H_2O$) and highly acidic H6–Y (6 H^+/sc) from Linde LZ-Y62 $[(NH_4)_{45}Na_{10}Al_{55}Si_{137}O_{384}]\cdot 235H_2O$. Heating the ammonium-exchanged zeolite under oxygen flow at 100 °C for 4 h and at 450 °C for 10 h and then under vacuum at the same temperature for 5 h (at a rate of 1 °C/min) resulted in the desired acid form. The dehydrated zeolites were kept in sealed vials in a glovebox prior to further treatments. The zeolites were loaded with an average of 0.8 molecules of $Cl_2(THF)GeM(CO)_5$ per supercage (determined by AAS) by stirring a slurry of 0.500 g of zeolite with the required amounts of complex **1** or **2** in 50 mL of pentane for 12 h under dry nitrogen atmosphere. The solvent was removed by vacuum filtration on a frit. The low loading level was chosen so that even a potential local attack at the framework will not lead to zeolite disintegration. All samples studied with EXAFS were heated at 50, 80, 100, 120, and 250 °C under vacuum for 10 h (at a heating rate of 1 °C/min). A color change from yellow to grey was generally observed at about 120 °C, indicating a major structural transition of the sample. In sample $Cl_2(THF)GeW(CO)_5$ in H6–Y, this transition was observed at about 150 °C. Samples were designated as follows: Na and H6 correspond to the zeolite form; e.g., H6 contains formally about 6 protons per supercage or 45 protons per unit cell. The temperatures of sample treatment are included in the affix of the sample name; e.g., GeMo(NaR) relates to $Cl_2(THF)GeMo(CO)_5$ in Na–Y at room temperature. GeW(H612) relates to $Cl_2(THF)GeW(CO)_5$ in H6–Y heated to 120 °C under vacuum.

Characterization of Zeolite Samples. *In Situ FTIR/TPD–MS.* FTIR data were taken with a Mattson Polaris spectrometer at 4-cm^{-1} resolution. Each sample was prepared as a thin dispersion on a Si wafer and introduced into a steel cell with CaF_2 windows under nitrogen atmosphere in a glovebox. The cell was connected to a turbomolecular pump combined with a quadrupole mass spectrometer (Dycor M200, 1–200 amu). Prepumping was achieved with molecular sieve pumps in order to eliminate hydrocarbon contamination. The residual H_2 pressure did not interfere with the measurements. The sample was evacuated until the total pressure (including H_2) was $<10^{-5}$ Torr prior to any treatment. Up to 5 mass fragments could be monitored as a function of time/temperature in the TPD-MS experiments. Zeolite samples were heated at 1 °C/min up to 300 °C, while the FTIR and mass spectra were continuously monitored.

EXAFS. EXAFS measurements were carried out at NSLS (Brookhaven National Laboratories) at beam line X-11A with a stored energy of 2.5 GeV and ring currents between 90 and 180 mA. The data were collected at the Ge K edge (11 103 eV) and the Mo K edge (20 000 eV) of the $Cl_2(THF)GeMo(CO)_5$ samples, and at the Ge edge and W L_3 edge (10 207 eV) of the $Cl_2(THF)GeW(CO)_5$ samples. The experiments were performed at about −170 °C in transmission using a double crystal Si(400) monochromator. The powdered samples were mixed in a glovebox under nitrogen atmosphere with a molten, degassed 1:1 mixture of octadecane and eicosane and mounted into EXAFS sample holders that were kept under nitrogen until the measurements were performed. The sample thickness was adjusted to a total absorption (μx) of about 2 units.

TABLE I: Crystallographic Data of Reference Compounds

reference compound	atom pair	R/Å	N	ref
$Mo(CO)_6$	Mo–*C*	2.058	6	*a*
	Mo–*CO*	3.206	6	
Na_2MoO_4	Mo–O	1.772	4	*b*
$MoSe_2$	Mo–Se	2.49	6	*c*
$MoCl_5$ (solid)	Mo–Cl	2.34	6	*d*
$W(CO)_6$	W–*C*	2.058	6	*a*
	W–*CO*	3.206	6	
Na_2WO_4	W–O	1.819	4	*b*
WSe_2	W–Se	2.49	6	*c*
WCl_6	W–Cl	2.26	6	*e*
GeO_2	Ge–O	1.88	6	*f*
$GeCl_4$	Ge–Cl	2.08	4	*g*
$Cl_2(THF)GeMo(CO)_5$	Ge–Mo	2.53	1	*h*

[a] Arnesen, S. P.; Seip, H. M. *Acta Chem. Scand.* **1966**, *20*, 2711. [b] Matsumoto, K.; Kobayashi, A.; Sasaki, Y. *Bull. Chem. Soc. Jpn.* **1975**, *48*, 1009. [c] James, P. J.; Lavik, M. T. *Acta Crystallogr.* **1963**, *16*, 1183. [d] Sands, D. E.; Zalkin, A. *Acta Crystallogr.* **1959**, *12*, 723. [e] Ewens, V. G.; Lister, M. W. *Faraday Soc. Trans.* **1938**, *34*, 1358. [f] Bauer, W. H.; Khan, A. *Acta Crystallogr.* **1971**, *B27*, 2133. [g] Bailar, J. C.; Emelens, H. J.; Nyholm, R.; Trotman-Dickinson, A. F. *Comprehensive Inorganic Chemistry*; Pergamon Press: Oxford, U.K., 1973; p 23. [h] (a) The distance is assumed to be equal to that of Ge=W in $(ArSe)_2(THF)GeW(CO)_5$ in b. (b) Behrens, H.; Moll, M.; Sixtus, E. *Z. Naturforsch.* **1977**, *32b*, 1105.

EXAFS Data Analysis. The EXAFS data were analyzed using standard procedures.[34] Phase functions and back-scattering amplitudes were extracted from appropriate references. The structural parameters of these reference compounds are summarized in Table I. Atomic background removal was achieved by employing a Victoreen curve to the pre-edge region and a cubic spline function to the EXAFS data. Normalization was performed using the step height of the absorption edge. References and samples were processed similarly to avoid artifacts.

EXAFS data of reference samples for the data analysis are shown in Figure 1 for the molybdenum edge, in Figure 2 for the tungsten edge, and in Figure 3 for the germanium edge. All spectra are displayed after performance of a background subtraction, normalization to a per atom basis, and Fourier transformation (FT). The magnitudes are an indication for coordination numbers, while the imaginary parts reflect the phase of the back-scattered photoelectron which is sensitive to the nature of the scattering ligand. Due to phase shifts, peak positions appear about 0.5-Å shorter than the true bond distances.

Results and Discussion

Structure of the Precursor $Cl_2(THF)GeMo(CO)_5$ (1). (*a*) *Mo Absorption Edge of 1.* The Fourier transformed Mo edge spectrum of precursor **1** is shown in Figure 4A. The ligand sphere of molybdenum in $Cl_2(THF)GeMo(CO)_5$ is similar to $Mo(CO)_6$, with the exception of the additional GeMo interaction. This is reflected in Figure 4A when compared to the reference $Mo(CO)_6$ in Figure 1A. Molybdenum hexacarbonyl contains two shells, one for the six carbon atoms at 2.058 Å (see Table I), which appear at ca. 1.5 Å in the phase-shift-uncorrected Fourier transformation, and one for the six oxygen atoms in the second neighbor shell at 3.206 Å (uncorrected at ca. 2.7 Å). The FT data of $Cl_2(THF)GeMo(CO)_5$ are similar in appearance but show an additional peak at ca. 2 Å. This intermediate peak is due to the Mo–Ge bond, which overlaps slightly with the oxygen contribution from the carbonyl ligand.

For quantitative analysis, the first shell of the sample was isolated by back-transforming it between 0.7 and 1.8 Å. Subsequently a fit was performed with the Mo–CO shell obtained from the EXAFS spectrum of $Mo(CO)_6$. The fit, which is shown in Figure 5A, results in a coordination number of 5.2 carbons and a bond distance of 2.05 Å (see Table II). Due to the interference of the Mo–Ge shell with the oxygen contribution of the carbonyl ligand, a successive fit had to be performed. To obtain the initial values for the oxygen shell, a back-transformation between 2.2

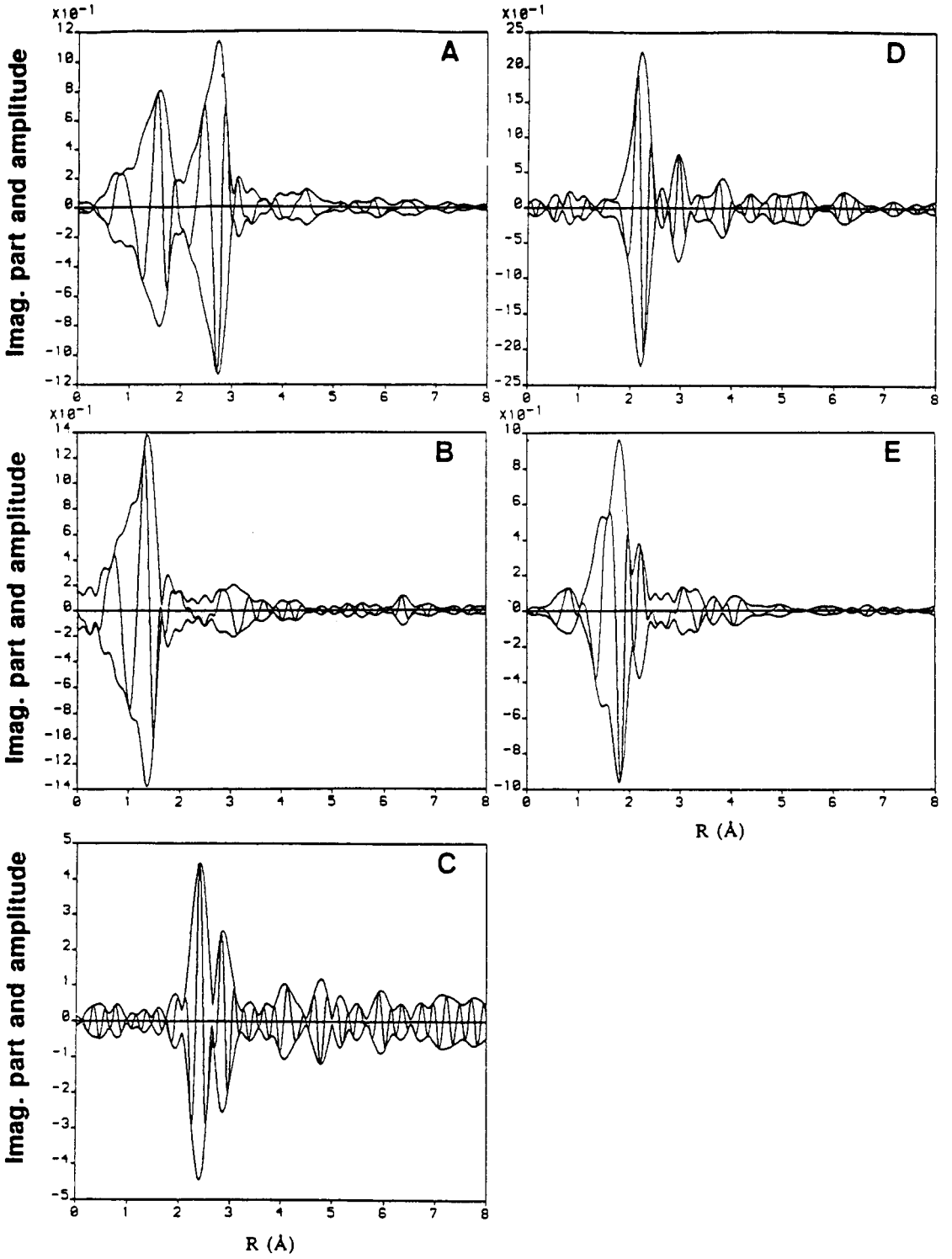

Figure 1. k^2 Fourier transformations of EXAFS references: (A) $Mo(C)_6$, (B) Na_2MoO_4, (C) Mo foil, (D) $MoSe_2$, (E) $(MoCl_5)_2$.

and 3.1 Å was applied to the outer shell, which was then fitted with a comparable data range of the $Mo(CO)_6$ reference. Subsequently, to analyze for the Mo–Ge contribution, the back-transform range was extended to 1.9–3.0 Å to combine both Mo–Ge and Mo–CO parts. The fit results using $MoSe_2$ and $Mo(CO)_6$ references reveal the presence of 1.0 Ge atom at a distance of 2.50 Å and 5.8 O atoms of the carbonyl ligand at 3.19 Å. The result is illustrated in Figure 5B. The deviation of the Mo–CO coordination from the expected value of 5.0 may be due to different M–C–O bond angles in the reference compound.

(*b*) *Ge Absorption Edge of 1.* The Fourier transformed spectrum of complex $Cl_2(THF)GeMo(CO)_5$ (**1**) at the Ge edge (Figure 4B) contains two different coordination spheres. A comparison of the imaginary part of the sample with references

TABLE II: EXAFS Fit Results for the Precursor $Cl_2(THF)GeMo(CO)_5$

sample	atom pair	N^a	R^b/Å	$\Delta\sigma^{2\,c}$/Å^2	ΔE^d/eV
		Mo Edge			
GeMo	Mo–CO	5.2	2.05	0.0002	−1.8
	Mo–*C*O	5.8	3.19	0.0023	−1.6
	Mo–Ge	1.0	2.50	−0.0019	−8.8
		Ge Edge			
GeMo	Ge–O	1.1	2.03	0.0063	0.5
	Ge–Cl	2.0	2.15	−0.0010	0.0
	Ge–Mo[e]	1.0	2.53		

[a] Coordination number. [b] Bond distance. [c] Static disorder. [d] Inner potential. [e] From an analogous structure in ref 35.

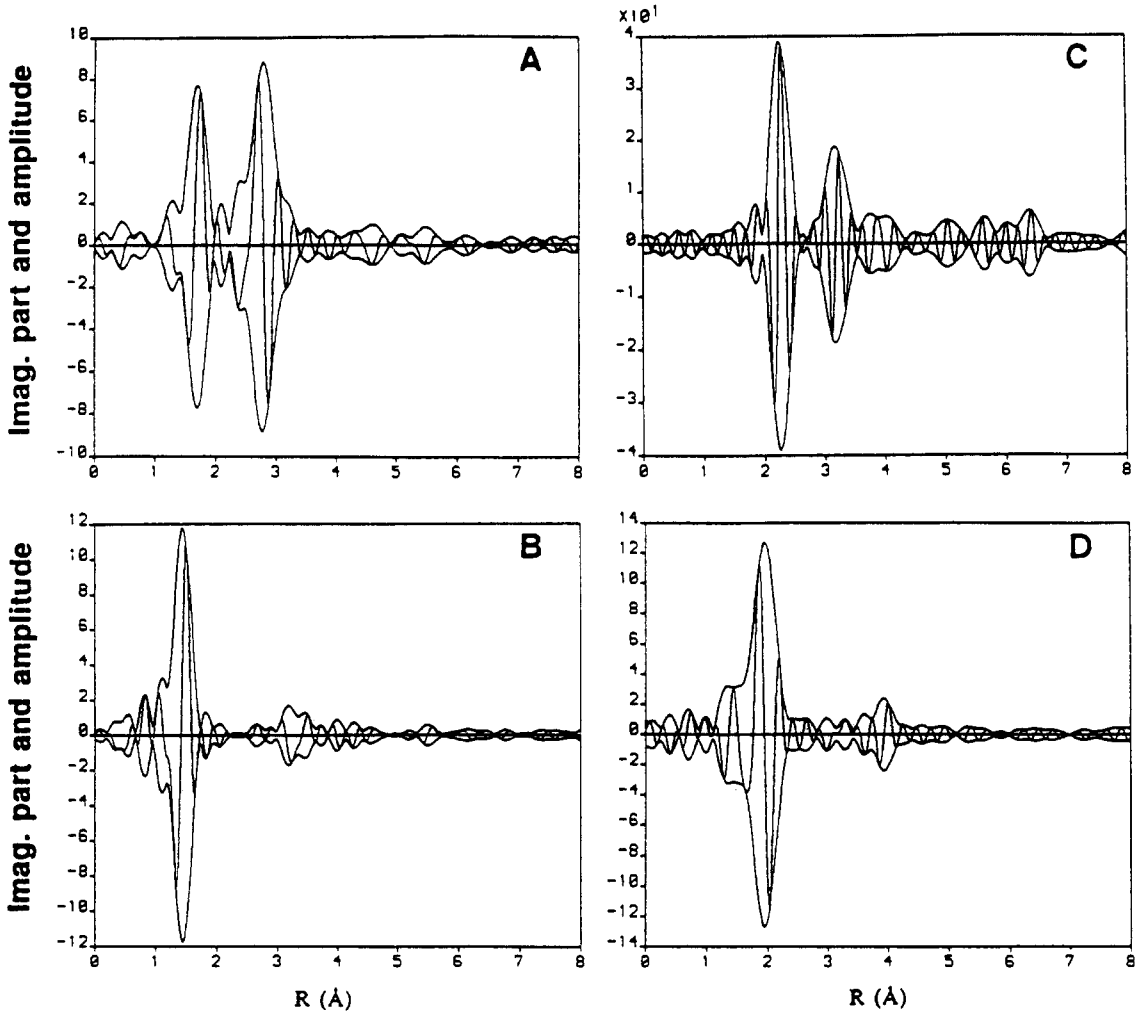

Figure 2. k^3 Fourier transformations of EXAFS references: (A) $W(CO)_6$, (B) Na_2WO_4, (C) WSe_2, (D) WCl_6.

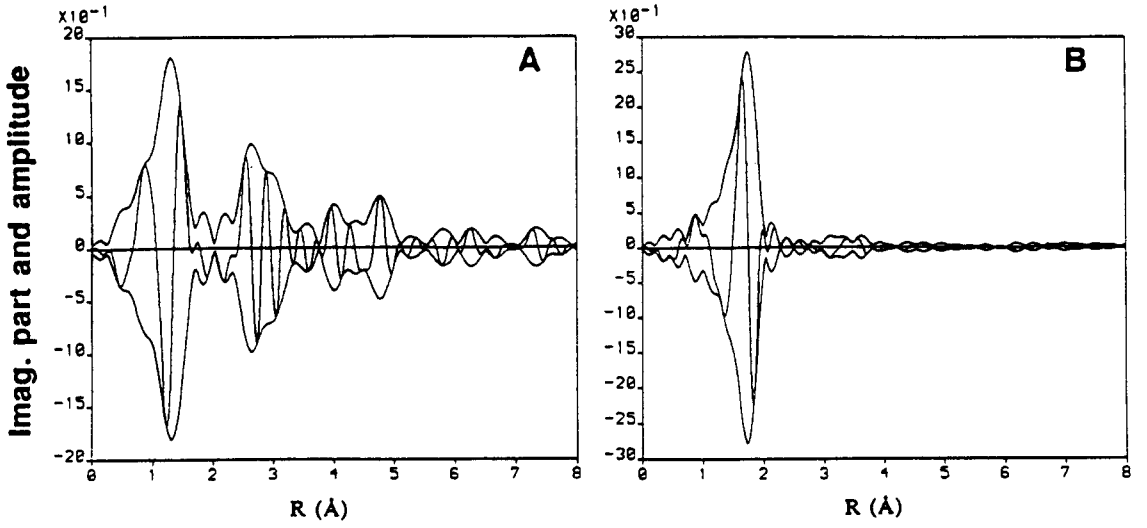

Figure 3. k^2 Fourier transformations of EXAFS references: (A) GeO_2, (B) $GeCl_4$.

GeO_2 and $GeCl_4$ (Figure 3A,B) indicates a strong resemblance to $GeCl_4$. The outer peak at about 2.3 Å coincides with the peak due to the Ge–Mo coordination in Figure 4B of the Mo edge data and is due to the same Ge–Mo contribution. An inverse Fourier transformation was applied over the range 0–2.1 Å to the first coordination sphere. A high quality fit was obtained consisting of two contributions: 2.0 Cl atoms at a distance R = 2.15 Å and 1.1 O atoms at R = 2.03 Å. The fit result is shown in Figure 5C. Combined EXAFS functions of O and Cl contributions were then calculated using the above fit results. They were subtracted from the original file, which was subsequently Fourier filtered resulting in the spectrum in Figure 5D. The envelope of this EXAFS function reveals that the outer shell in Figure 4B definitely belongs to a heavy atom scatterer; this is consistent with the Ge–Mo coordination. An adequate reference to analyze this contribution was not available, but it was used as an internal standard for analysis of all other zeolite samples. Recently, the crystal structure of an analogous compound $(ArSe)_2Ge{=}W(CO)_5$ was reported[35] with a Ge=W distance of 2.53 Å. This bond length coincides with that determined from the Mo edge data (2.50 Å) of $Cl_2(THF)GeMo(CO)_5$ and is used for all further fits. The above results, summarized in Table II, show that the molecular

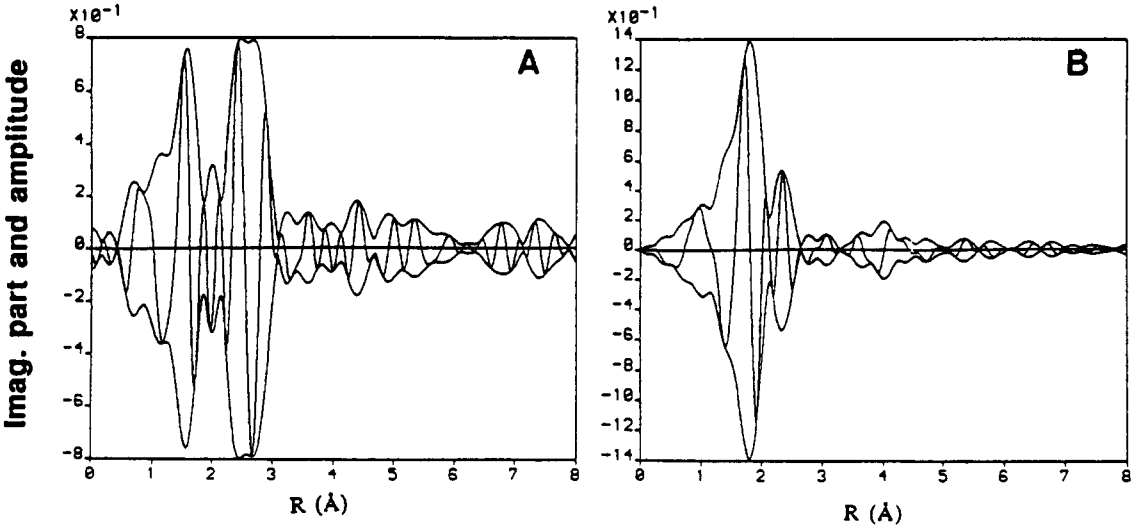

Figure 4. Fourier transformations of EXAFS samples, $Cl_2(THF)GeMo(CO)_5$ precursor: (A) Mo edge spectra, FT = k^2, 3.2–13 Å^{-1}, at room temperature; (B) Ge edge spectra, FT = k^2, 2.6–13 Å^{-1}, at room temperature.

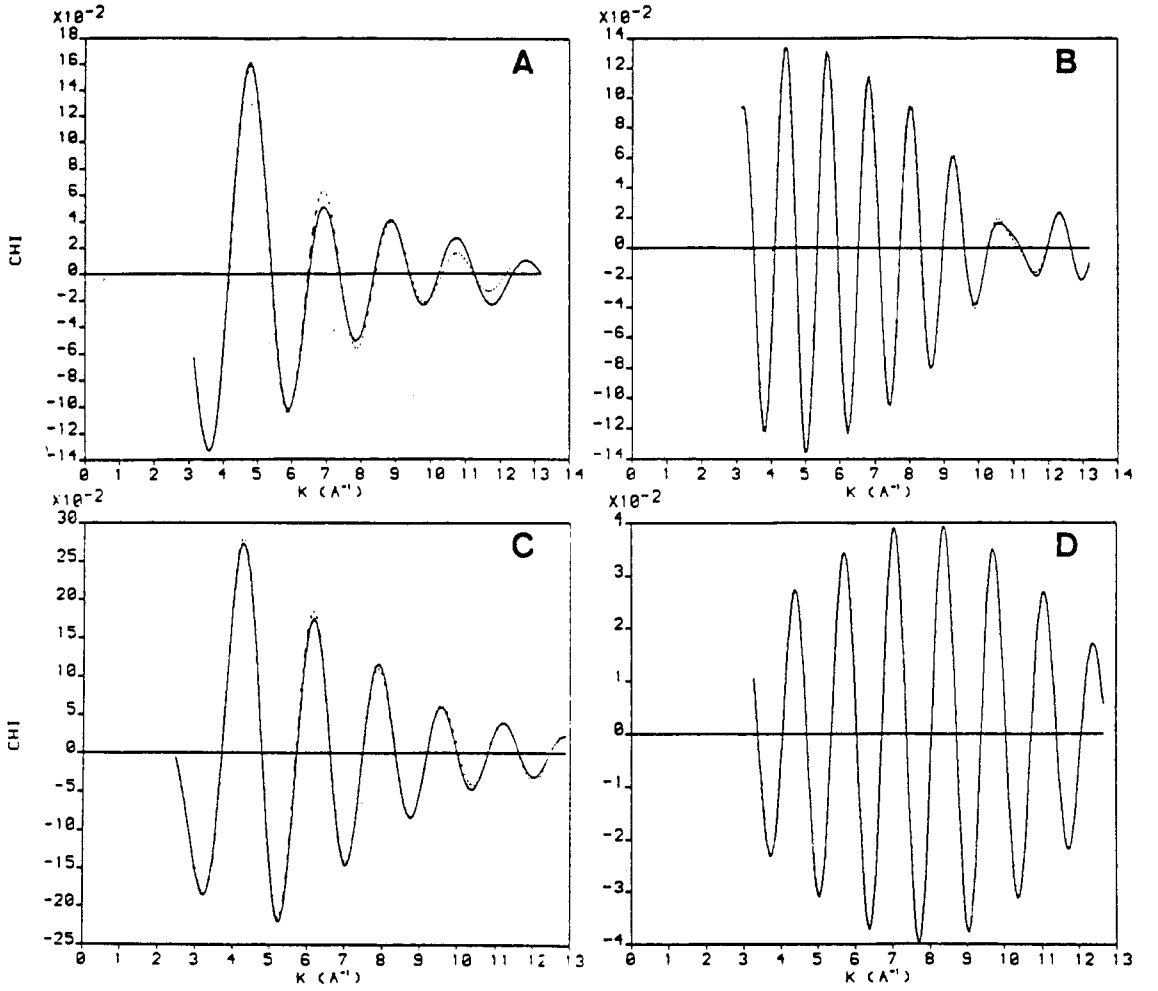

Figure 5. Fit results of the back-transformed EXAFS data of $Cl_2(THF)GeMo(CO)_5$ precursor, original data (solid line) and fit (dotted line). Mo edge: (A) of Mo–CO contribution, (B) of Mo–*C*O and Mo–Ge contributions. Ge edge: (C) of Ge–O and Ge–Cl contributions, (D) back-transformed data of Ge–Mo contribution without fitting.

structure of complex **1** is consistent with the structure of its analogs.[36] Similar analytical procedures as described for the precursor were used for both Mo and Ge absorption edge spectra of all other samples.

Structure and Stability of $Cl_2(THF)GeMo(CO)_5$ Adsorbed in Na–Y. (*a*) *Mo Absorption Edge Data of 1 in Na–Y.* The spectrum of $Cl_2(THF)GeMo(CO)_5$ in Na–Y at room temperature (GeMo(NaR); Figure 6A) shows imaginary parts similar to that of the precursor **1** except with a reduction in the Mo–Ge contribution. Data analysis of sample GeMo(NaR) shows the presence of three to four carbons at a distance of 2.05 Å. A bond distance of 3.16 Å is found for Mo–C*O*, and 2.48 Å for 0.6 Ge atoms (see Table III). With the sample being heated to 50, 80, 100, 120 and 250 °C, carbonyl intensities decrease drastically (starting at 80 °C), while the Mo–Ge bond survives to about 100 °C. The decomposition of the precursor in Na–Y starts at this temperature, as evident from a strongly reduced Mo–Ge contribution at the Ge edge (not shown). The overall change is most

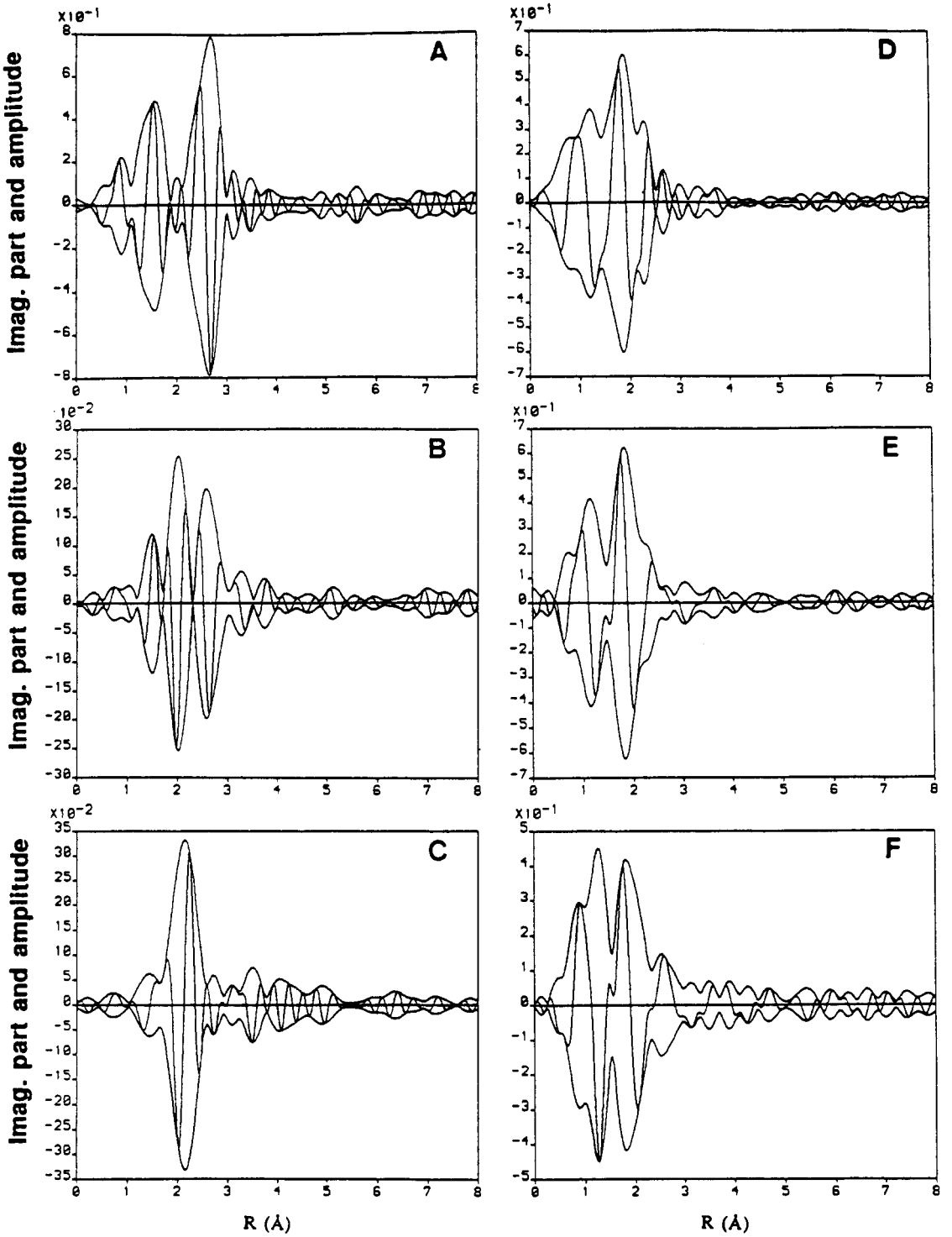

Figure 6. Fourier transformations of EXAFS samples, $Cl_2(THF)GeMo(CO)_5$ in Na–Y. Mo edge spectra: (A) FT = k^2, 3.3–13 Å^{-1}, at room temperature; (B) FT = k^2, 3.3–12 Å^{-1}, at 120 °C; (C) FT = k^2, 3.3–12 Å^{-1}, at 250 °C. Ge edge spectra: FT = k^2, 2.7–13 Å^{-1}, at room temperature; (E) FT = k^2, 2.7–13 Å^{-1}, at 120 °C; (F) FT = k^2, 2.7–12 Å^{-1}, at 250 °C.

obvious at 120 °C (Figure 6B); the first and outer shells still represent the CO ligands at much reduced intensity. A dominant shell appears at about 2 Å, which differs from the Ge–Mo contribution at room temperature.[37] This shell is due to unidentified $MoCl_x$ species. At 250 °C, the CO ligands have vanished and chloride coordination remains at the Mo center.

(*b*) *Ge Absorption Edge of 1 in Na–Y.* When the precursor **1** is introduced into Na–Y at room temperature, the FT spectrum at the Ge edge (Figure 6D) broadens compared to the nonsupported precursor. At a distance of 2.22 Å, 1.1 chlorine atoms are found in addition to disordered oxygen at a mean distance of 1.99 Å (Table III). The reduced chloride coordination suggests that the precursor **1** begins to attach to the zeolite framework already at room temperature. Very similar coordination data were obtained up to 80 °C. At 100 °C, the Ge–Mo contribution is reduced remarkably, and at 250 °C, it disappears. At 120 °C (Figure 6E), the chloride coordination is almost unchanged from that of the room temperature sample (1.2 Cl at 2.20 Å). At 250 °C (Figure 6F) chloride is still present and 2.6 oxygen atoms are located at 1.97 Å. A small peak at ca. 2.5 Å (uncorrected), assigned to framework Si/Al, is now more visible than at room temperature.

From the above data of **1** in Na–Y, it can be concluded that the attachment of the precursor complex to the zeolite framework via the Ge moiety starts already at room temperature by substitution for one chloride ion. The second chloride remains at-

TABLE III: EXAFS Fit Results for $Cl_2(THF)GeMo(CO)_5$ in Zeolite Na-Y

sample	atom pair	N^a	R^b/Å	$\Delta\sigma^{2c}$/Å^2	ΔE^d/eV
		Mo Edge			
GeMo(NaR)	Mo–CO	3.5	2.05	0.0000	−1.5
	Mo–*C*O	4.4	3.16	0.0039	−0.9
	Mo–Ge	0.6	2.48	−0.0037	−7.1
GeMo(Na12)	Mo–CO	0.6	2.08	−0.0009	−2.6
	Mo–*C*O	1.0	3.14	0.0002	0.4
	Mo–Cl	1.4	2.53	−0.0023	−5.5
GeMo(Na25)	Mo–O	0.2	2.04	0.0004	7.9
	Mo–Cl	3.6	2.63	0.0027	10.8
	Mo–Cl	1.3	2.95	0.0000	−3.0
		Ge Edge			
GeMo(NaR)	Ge–O	2.3	1.99	0.0151	0.0
	Ge–Cl	1.1	2.22	0.0026	1.1
	Ge–Mo	0.6	2.53	0.0014	0.4
GeMo(Na12)	Ge–O	2.8	1.96	0.0131	−4.6
	Ge–Cl	1.2	2.20	0.0007	4.7
GeMo(Na25)	Ge–O	2.6	1.97	0.0073	−5.7
	Ge–Cl	1.2	2.21	0.0038	5.1

[a] Coordination number. [b] Bond distance. [c] Static disorder. [d] Inner potential.

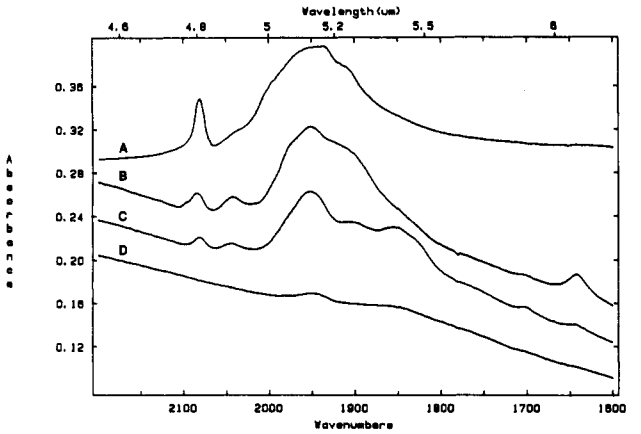

Figure 7. In situ FTIR spectra of $Cl_2(THF)GeMo(CO)_5$: (A) in KBr, (B) in Na-Y at room temperature, (C) in Na-Y at 60 °C, (D) in Na-Y at 90 °C.

tached to the Ge atom even at 250 °C. The Ge–Mo bond is fairly stable up to ca. 100 °C, while complex decomposition and formation of molybdenum chloride species occurs at higher temperatures.

In Situ FTIR/TPD-MS Data for 1 in Na-Y. The IR spectra of $Cl_2(THF)GeMo(CO)_5$ in KBr and Na-Y are shown in Figure 7. The carbonyl ligands of the precursor in KBr (top spectrum) show three bands at 2082 (m), 1947 (vs, br), and 1908 (sh) cm^{-1}. After introducing complex **1** into Na-Y, the in situ IR spectrum shows four major CO bands at 2085 (w), 2043 (w), 1951 (vs, br), and 1904 (sh) and a minor band at 1642 (w) cm^{-1} (no water is present in the zeolite as there are no OH stretch vibrations around 3500 cm^{-1}). The split of the higher frequency band indicates a lower symmetry of the molybdenum carbonyl moiety in Na-Y, due to an interaction between carbonyls and sodium in the zeolite framework which is also observed, for example, with intrazeolite $Ni(CO)_4$.[11]

Upon being heated to 60 °C, two additional bands appear at 1904 and 1852 cm^{-1} while the band at 1642 cm^{-1} has almost vanished. The lower frequency bands are assigned to molybdenum fragments with less than five carbonyls. This is consistent with the reduced CO coordination number as found in the EXAFS analysis. All carbonyls have almost disappeared at 90 °C.[38] Simultaneous detection of species desorbed from the zeolite samples was carried out by mass spectrometry. A TPD-MS profile is shown in Figure 8. Carbonyl fragments (mass 28) appear in the mass spectrum at ca. 50 °C and reach a maximum at 67 °C. These observations are in agreement with the IR results discussed above. No HCl or any metal carbonyl fragments were detected in the TPD-MS profile.

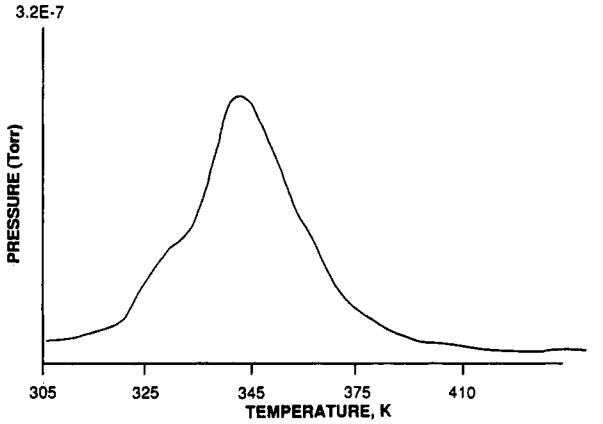

Figure 8. TPD-MS profile of $Cl_2(THF)GeMo(CO)_5$ in Na-Y, measured simultaneously with the FTIR spectra in Figure 7: CO (mass 28).

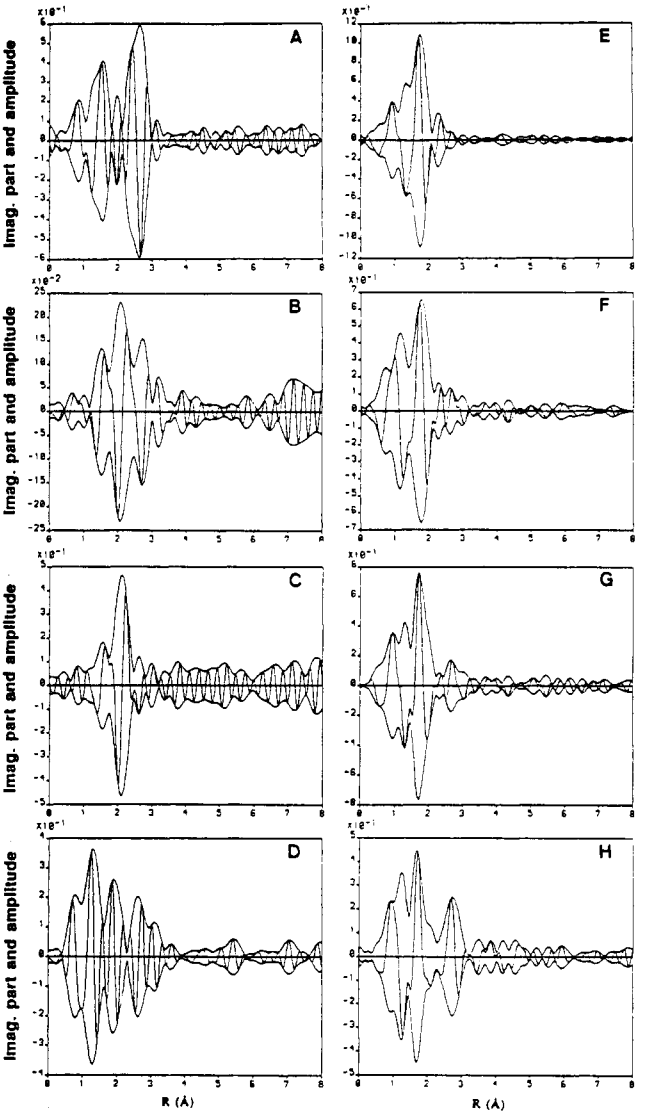

Figure 9. Fourier transformations of EXAFS samples $Cl_2(THF)GeMo(CO)_5$ in H6-Y. Mo edge spectra: (A) FT = k^2, 3.3–13 Å^{-1}, at room temperature; (B) FT = k^2, 3.3–13 Å^{-1}, at 100 °C; (C) FT = k^2, 3.3–13 Å^{-1}, at 120 °C; (D) FT = k^2, 3.8–12 Å^{-1}, at 250 °C. Ge edge spectra: (E) FT = k^2, 2.7–13 Å^{-1}, at room temperature; (F) FT = k^2, 2.7–13 Å^{-1}, at 100 °C; (G) FT = k^2, 2.7–13 Å^{-1}, at 120 °C; (H) FT = k^2, 2.7–11 Å^{-1}, at 250 °C.

Structure and Stability of $Cl_2(THF)GeMo(CO)_5$ Adsorbed in H6-Y. (*a*) *Mo Absorption Edge of 1 in H6-Y.* The Mo FT spectra of the precursor $Cl_2(THF)GeMo(CO)_5$ in H6-Y zeolite

TABLE IV: EXAFS Fit Results for $Cl_2(THF)GeMo(CO)_5$ in Zeolite H6-Y

sample	atom pair	N^a	R^b/Å	$\Delta\sigma^{2c}$/Å^2	ΔE^d/eV
		Mo Edge			
GeMo(H6R)	Mo–CO	3.0	2.04	0.0009	−0.9
	Mo–C*O*	3.9	3.17	0.0018	0.4
	Mo–Ge	0.6	2.46	−0.0013	4.1
GeMo(H610)	convolution of all shells, but similar to GeMoNa12				
GeMo(H612)	Mo–Mo	1.1	1.93	0.0133	4.8
	Mo–Cl	3.6	2.61	0.0002	−10.5
GeMo(H625)	Mo–O	0.7	1.72	−0.0045	−1.6
	Mo–Mo	0.5	2.19	0.0031	−4.6
	Mo–Mo	0.7	3.01	0.0015	7.0
		Ge Edge			
GeMo(H6R)	Ge–O	1.7	2.00	0.0088	−1.3
	Ge–Cl	1.6	2.15	0.0002	0.5
	Ge–Mo	0.7	2.52	0.0020	3.6
GeMo(H610)	Ge–O	2.0	1.92	0.0141	2.5
	Ge–Cl	1.1	2.18	0.0010	−0.3
	Ge–Mo	0.3	2.52	0.0003	−0.5
GeMo(H612)	Ge–O	2.5	2.03	0.0149	−7.2
	Ge–Cl	1.1	2.15	0.0002	6.7
GeMo(H625)	Ge–O	2.0	1.98	0.008	−4.8
	Ge–Cl	1.1	2.17	0.001	8.8
	outer shell:	Si/Al			
alternative possible	Ge–O	1.3	1.94	0.0004	−5.4
fit:	Ge–O	2.4	2.14	−0.0004	−1.4

[a] Coordination number. [b] Bond distance. [c] Static disorder. [d] Inner potential.

at room temperature and 100, 120, and 250 °C are shown in Figure 9A–D. The sample at room temperature shows a slightly more resolved Mo–Ge shell than the one in Na–Y, due to less intense carbonyl peaks (on average about 3.5 CO ligands instead of 4 in Na–Y; Table IV). The FT spectrum of the sample at 120 °C is comparable to that of Na–Y at 250 °C. No Mo–Ge interaction and no carbonyl remain at 120 °C. A new Mo–Mo interaction with a bond distance of 1.93 Å is indicated. This short Mo–Mo bond distance is fairly close to that of Mo–Mo quadruple bonds (2.09 Å for Mo_2ac_4).[39] A second shell could be fitted with three chloride ligands at 2.61 Å, indicating unknown $MoCl_x$ products. On the basis of mass balance, three Cl per Mo are not possible; a nonresolved convolution with Mo–oxygen or other coordination (for instance from MoO_xCl_y species) may be present. The short Mo–Mo bond is retained in the sample at 250 °C (see Figure 9D). The first shell in this sample originates from a Mo–O interaction (N = 0.7, R = 1.72 Å) which is accompanied by a Si/Al peak at ca. 3.2 Å (see Table IV).

(*b*) *Ge Absorption Edge of* **1** *in H6–Y.* The spectrum of the GeMo(H6R) sample at room temperature is comparable to that of the intact precursor, with the exception of a smaller Ge–Mo shell and partial replacement of chloride by oxygen. The fit results show the average presence of 1.7 oxygens at Ge–O = 2.00 Å, 1.6 chlorides at Ge–Cl = 2.15 Å, and 0.7 molybdenum atom at Ge–Mo = 2.52 Å. Upon being heated, the chloride coordination steadily decreases accompanied by an increase in oxygen coordination. Finally, at 250 °C, a Si/Al contribution emerges (Figure 9H). The Ge–Mo bond vanishes between 100 and 120 °C.

Together with the results from the Mo edge analysis, it can be concluded that the precursor **1** attaches to the H6–Y zeolite framework, increasingly with rising temperature, until decomposition begins between 100 and 120 °C. After the Ge–Mo bond is broken, multiply bonded Mo–Mo species are formed. Germanium chloride species remain attached to the zeolite framework at high temperature.

In Situ FTIR/TPD–MS of 1 in H6–Y. The FTIR spectra of $Cl_2(THF)GeMo(CO)_5$ in KBr and H6–Y are shown in Figure 10. As in NaY, the carbonyl band at higher frequency splits into two bands at 2085 and 2050 cm^{-1} when **1** is adsorbed into the H6–Y support. In contrast to Na–Y, the only other prominent band appears at 1964 cm^{-1}. Because the structural features of these samples are comparable, the differences in vibrational

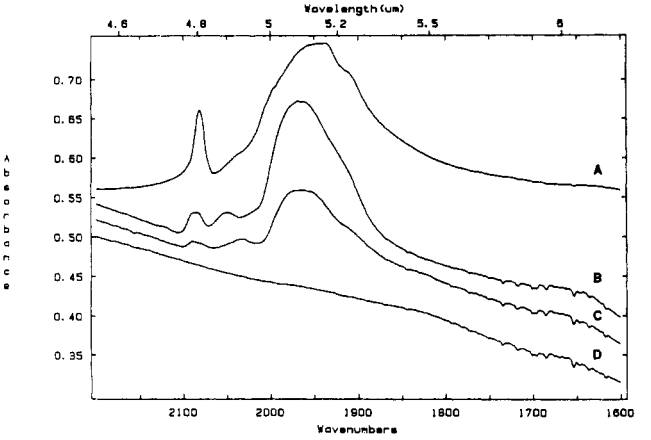

Figure 10. In situ FTIR spectra of $Cl_2(THF)GeMo(CO)_5$: (A) in KBr, (B) in H6–Y at room temperature, (C) in H6–Y at 60 °C, (D) in H6–Y at 90 °C.

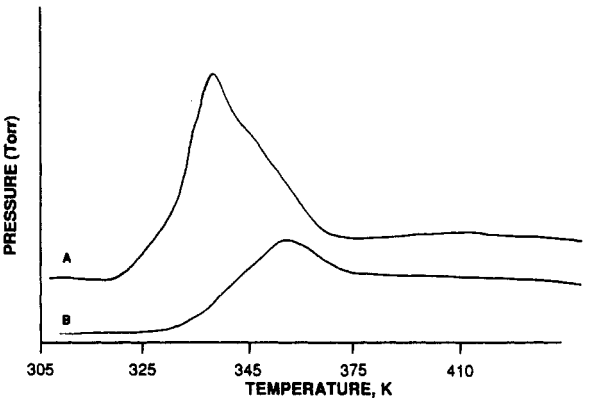

Figure 11. TPD-MS profiles of $Cl_2(THF)GeMo(CO)_5$ in H6–Y, measured simultaneously with the FTIR spectra in Figure 10: (A) CO (mass 28); (B) HCl (mass 36), enlarged 35×.

characteristics must originate from subtle symmetry changes due to absorption in the zeolite. The Na ions that cause more drastic distortions in Na–Y are not present in H6–Y. Decarbonylation of the sample (in a thin dispersion on a Si wafer) occurs between ca. 40 and 90 °C, and a maximum of CO loss can be seen at 65 °C in the TPD–MS profile (Figure 11). A trace amount of HCl (mass 36) was detected with a maximum at about 80 °C. This observation confirms the anchoring process via removal of HCl as deduced from the EXAFS data.

Structure and Stability of $Cl_2(THF)GeW(CO)_5$ (2) Adsorbed in Na–Y. (*a*) *W Absorption Edge of* **2** *in Na–Y.* In general, the intrazeolite chemistry of the Mo and W complexes is similar, but differences in stability are observed which might be advantageous for later applications of these systems. Figure 12 displays Fourier transformed EXAFS spectra of **2** in Na–Y (sample GeW(Na–Y)) at the W edge (a–c) and of corresponding spectra at the Ge edge (d–f) at room temperature and 120 and 250 °C. The imaginary parts in $W(CO)_6$ (Figure 2A) and in **2** (Figure 12A) resemble each other in the carbon and oxygen contributions of the carbonyl ligands. Data analysis of sample GeW(NaR) results in 5.1 CO at 2.03 Å (Table V, Figure 13). In addition, a third component due to W–Ge at 2.53 Å (0.8 Ge atom) is visible between both shells. These data show that the tungsten coordination sphere is retained upon adsorption in Na–Y.

Samples heated at 50, 80, and 100 °C show essentially no changes in the EXAFS, compared to those at room temperature (see Table V). However, drastic structural changes occur between 100 and 120 °C. The carbonyl coordination reduces to 2.1 per W with a shortened bond of 1.98 Å (Figure 12B). A new strong band now overlaps with the carbon contribution of the carbonyl. It was found to consist of 2.5 chlorides at 2.41 Å. The presence of the chloride peak indicates the formation of (unidentified) WCl_x species upon decomposition of intrazeolite **2**.

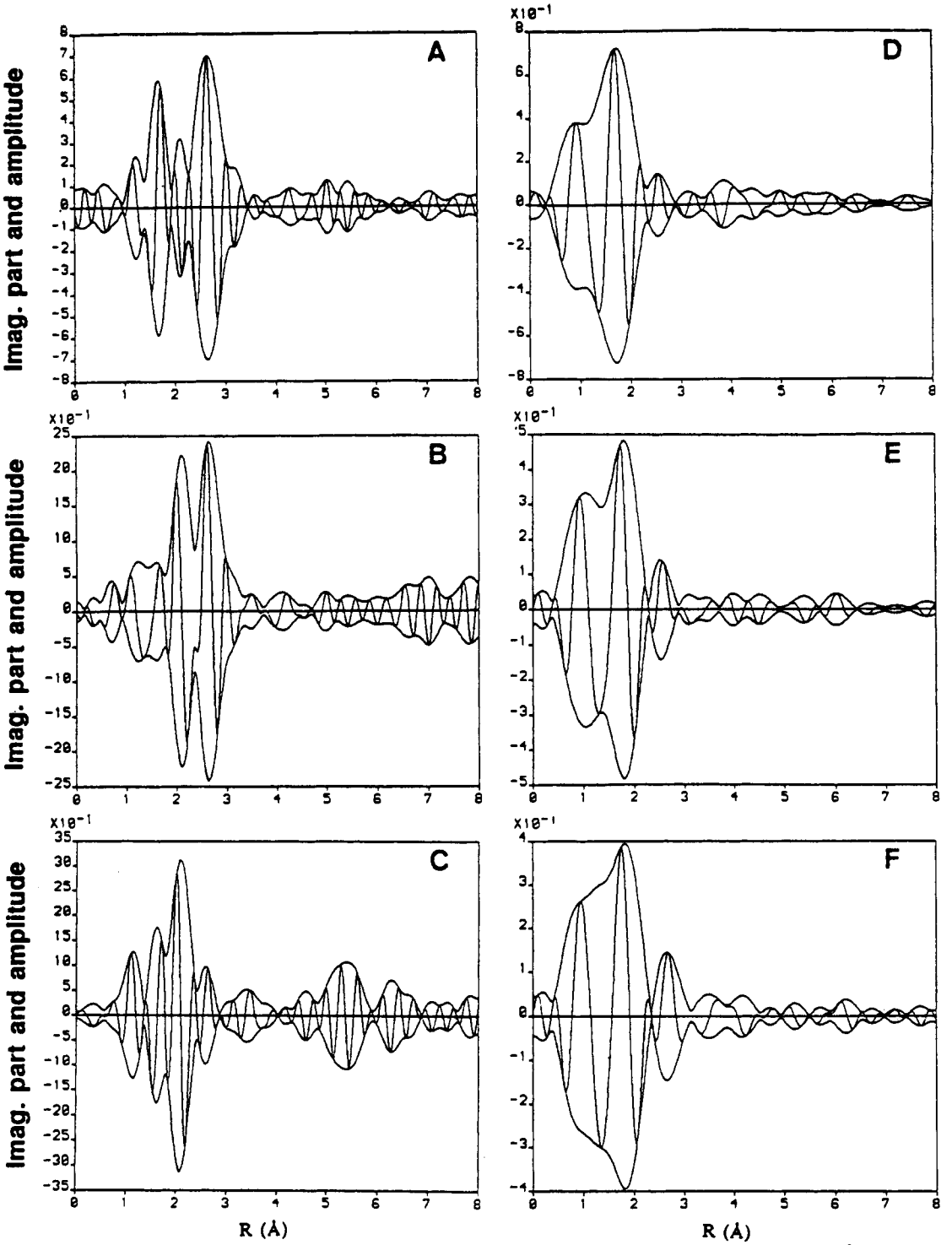

Figure 12. Fourier transformations of EXAFS samples, $Cl_2(THF)GeW(CO)_5$ in Na–Y. W edge spectra: (A) FT = k^3, 2.6–12 Å^{-1}, at room temperature; (B) FT = k^3, 2.6–12 Å^{-1}, at 120 °C; (C) FT = k^3, 2.6–12 Å^{-1}, at 250 °C. Ge edge spectra: (D) FT = k^2, 2.7–9 Å^{-1}, at room temperature; (E) FT = k^2, 2.7–9 Å^{-1}, at 120 °C; (F) FT = k^2, 2.7–9 Å^{-1}, at 250 °C.

Further changes are visible after heating to 250 °C. The oxygen of the carbonyl ligand has vanished, leaving the chloride peak dominant in the spectrum. A fit of this contribution with WCl_6 and subsequent inclusion of the peak at ca. 1.8 Å results in 3 chlorine ligands with a W–Cl bond of 2.40 Å and an additional contribution of 0.8 oxygen at 2.04 Å. This oxygen ligand in addition to a small outer peak at ca. 2.8 Å (uncorrected for phase shift) may indicate a weak coordination of WCl_x species to the framework of the zeolite. As in the case of $MoCl_x$ in the H6–Y host, mass balance does not allow WCl_3, and convolution with other coordination is likely.

Having established that the carbonyl coordination sphere and the W–Ge bond of the $Cl_2(THF)GeW(CO)_5$ precursor are stable to at least 100 °C within zeolite Na–Y, it is interesting to study if the germanium moiety can be attached to the zeolite lattice. This issue was explored at the Ge absorption edge.

(b) Ge Absorption Edge of 2 in Na–Y. One broad peak is observed in the Ge edge FT spectrum of $Cl_2(THF)GeW(CO)_5$ in Na–Y at room temperature (Figure 12D). As in the case of the GeMo complex, oxygen coordination is increased and chloride coordination decreased in this sample (1.9 oxygen atoms at 1.93 Å and 1.5 chlorine atoms at 2.19 Å; Table VI). When the sample is heated to 100 and 250 °C, the EXAFS data show a decrease from 1.5 to 1 chloride atoms, accompanied by an increase from 1.9 to 2.6 oxygen atoms. At the same time we notice the growth of a peak at about 2.6 Å, which is most prominent at 250 °C, but already present at room temperature (Si/Al). These observations indicate an attachment of the germanium to the zeolite lattice.

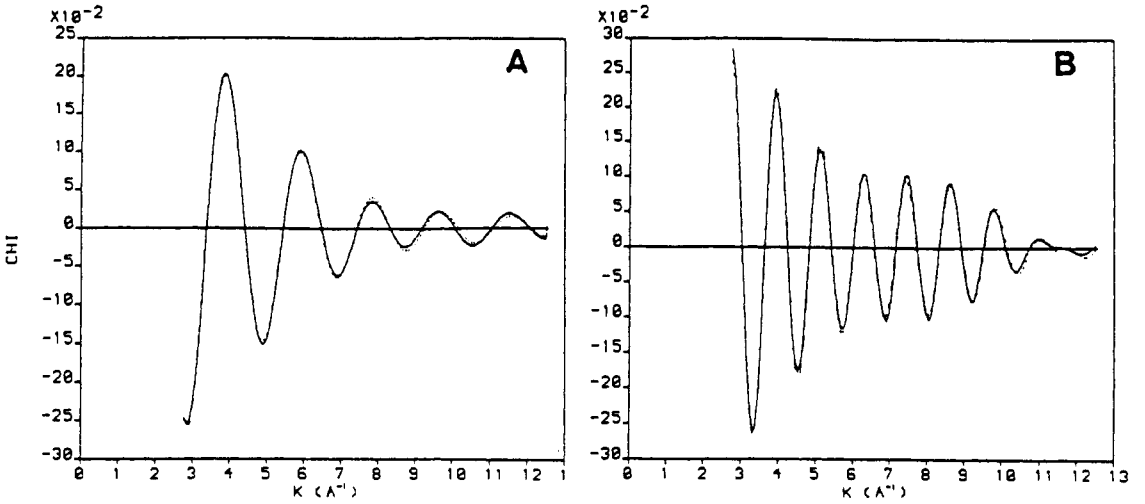

Figure 13. Sample GeW(NaR), fit results of the W edge: (A) back-transformation of the W–*C*O contribution, original data (solid line) and fit (dotted line); (B) back-transformation of W–*C*O and W–Ge contributions, original data (solid line) and fit (dotted line). Note: The W–Ge contribution is visible in the nonexponential decay of the amplitude function.

TABLE V: EXAFS Fit Results for $Cl_2(THF)GeW(CO)_5$ in Zeolite Na–Y

sample	atom pair	N^a	R^b/Å	$\Delta\sigma^{2c}$/Å^2	ΔE^d/eV
		W Edge			
GeW(NaR)	W–*C*O	5.1	2.03	0.0007	2.1
	W–C*O*	5.5	3.18	0.0014	0.1
	W–Ge	0.8	2.53	–0.0001	10.4
GeW(Na10)	W–*C*O	5.1	2.02	0.0019	1.3
	W–C*O*	5.5	3.18	0.0010	0.6
	W–Ge	0.8	2.54	0.0024	–8.8
GeW(Na12)	W–*C*O	2.1	1.98	0.0029	–1.1
	W–C*O*	2.3	3.09	0.0013	5.0
	W–Cl	2.5	2.41	0.0041	–3.3
GeW(Na25)	W–O	0.8	2.04	–0.0001	–4.4
	W–Cl	3.0	2.40	0.0041	1.9
		Ge Edge			
GeW(NaR)	Ge–O	1.9	1.93	0.0037	6.7
	Ge–Cl	1.5	2.19	0.0014	–2.9
GeW(Na10)	Ge–O	1.9	1.97	0.0057	0.1
	Ge–Cl	1.2	2.20	0.0017	–3.2
GeW(Na12)	Ge–O	2.3	1.96	0.0146	0.4
	Ge–Cl	1.1	2.22	0.0036	–2.9
GeW(Na25)	Ge–O	2.6	2.04	0.0164	–5.0
	Ge–Cl	1.0	2.26	0.0060	–1.3

[a] Coordination number. [b] Bond distance. [c] Static disorder. [d] Inner potential.

TABLE VI: EXAFS Fit Results for $Cl_2(THF)GeW(CO)_5$ in H6–Y

sample	atom pair	N^a	R^b/Å	$\Delta\sigma^{2c}$/Å^2	ΔE^d/eV
		W Edge			
GeW(H6R)	W–*C*O	4.6	2.03	0.0012	1.0
	W–C*O*	4.9	3.18	0.0004	0.6
	W–Ge	0.7	2.53	0.0022	–13.0
GeW(H612)	W–*C*O	4.1	2.04	0.0003	0.0
	W–C*O*	4.1	3.17	0.0010	0.5
	W–Ge	0.8	2.54	0.0028	–10.0
GeW(H615)	W–O	0.9	1.84	0.0044	3.5
	W–Cl	4.1	2.33	0.0130	3.5
GeW(H625)	W–O	1.9	1.81	0.0105	6.3
	W–Cl	2.9	2.34	0.0116	1.0
		Ge Edge			
GeW(H6R)	Ge–O	1.3	1.98	0.0007	3.3
	Ge–Cl	2.1	2.15	0.0016	–0.3
GeW(H612)	Ge–O	1.5	2.02	0.0053	–2.6
	Ge–Cl	1.7	2.14	0.0023	4.3
GeW(H615)	Ge–O	more than one shell			
	Ge–Cl	1.4	2.19	0.0081	1.0
GeW(H625)	Ge–O	3.6	2.03	0.0120	0.0
	Ge–Cl	1.2	2.17	0.0040	10.3

[a] Coordination number. [b] Bond distance. [c] Static disorder. [d] Inner potential.

This process starts upon adsorption of the complex into the framework at room temperature.

Structure and Stability of $Cl_2(THF)GeW(CO)_5$ Adsorbed in H6–Y. (*a*) *W Absorption Edge of 2 in H6–Y.* The W edge EXAFS FT spectra for sample $Cl_2(THF)GeW(CO)_5$ in H6–Y are shown in Figure 14A–D, at room temperature and 120, 150, and 250 °C, respectively. In contrast to the Na–Y host, *in H6–Y the overall features of the complex are retained at 120 °C (Figure 14B).* The slight decrease of the CO coordination is reflected in an average coordination number of 4, but the Ge–W bond is kept mostly intact (N = 0.8, R = 2.54 Å; Table VI). At 150 °C, the Ge–W bond is destroyed and chloride reacts with W to form WCl_x species. Higher temperatures increase the W–zeolite coordination (250 °C: 1.9 oxygens at 1.81 Å and Si/Al).

(*b*) *Ge Absorption Edge of 2 in H6–Y.* At room temperature, the Ge coordination shell resembles that of the precursor (Table VI). No outer shell as in the Na–Y host is observed. Together with the information of the tungsten edge data, it can be concluded that the precursor is unchanged at this temperature in zeolite H6–Y. No significant attachment to the zeolite matrix has taken place. At higher temperature a slow increase in the oxygen coordination and a concomitant decrease of chloride occurs. An outer shell due to zeolite coordination becomes visible at about 2.6 Å (uncorrected for phase shift). This process starts at 80 °C and ends with an average Ge coordination of 3.6 oxygens (disordered) at 2.03 Å and 1.2 chlorides at 2.17 Å, at 250 °C.

In situ FTIR spectra in Figure 15 of the $Cl_2(THF)GeW(CO)_5$ complex in H6–Y show a carbonyl pattern that closely resembles the one of the precursor in KBr, with the main peaks at 1946, 1980, and 2085 cm^{-1}. In agreement with the EXAFS data, the CO intensities remain constant until an abrupt decrease occurs at 130 °C, leaving no trace of CO at 150 °C. TPD-MS data of the evolving gases from the IR dispersion (Figure 16), indicate a maximum release of CO at 130 °C. A small amount of HCl which increased at higher temperature was detected at the same time (note: scale is expanded 10 times). This corresponds to the removal of chloride ligands derived from the EXAFS data between 150 and 250 °C.

Conclusion

Combined EXAFS data of two absorption edges and in situ FTIR measurements with TPD-MS data proved valuable in elucidating the intrazeolite structure and stability of the bimetallic precursor complexes $Cl_2(THF)GeMo(CO)_5$ and $Cl_2(THF)GeW(CO)_5$. It could be shown that the stability range of the complexes included in zeolites of different surface acidity is similar to the

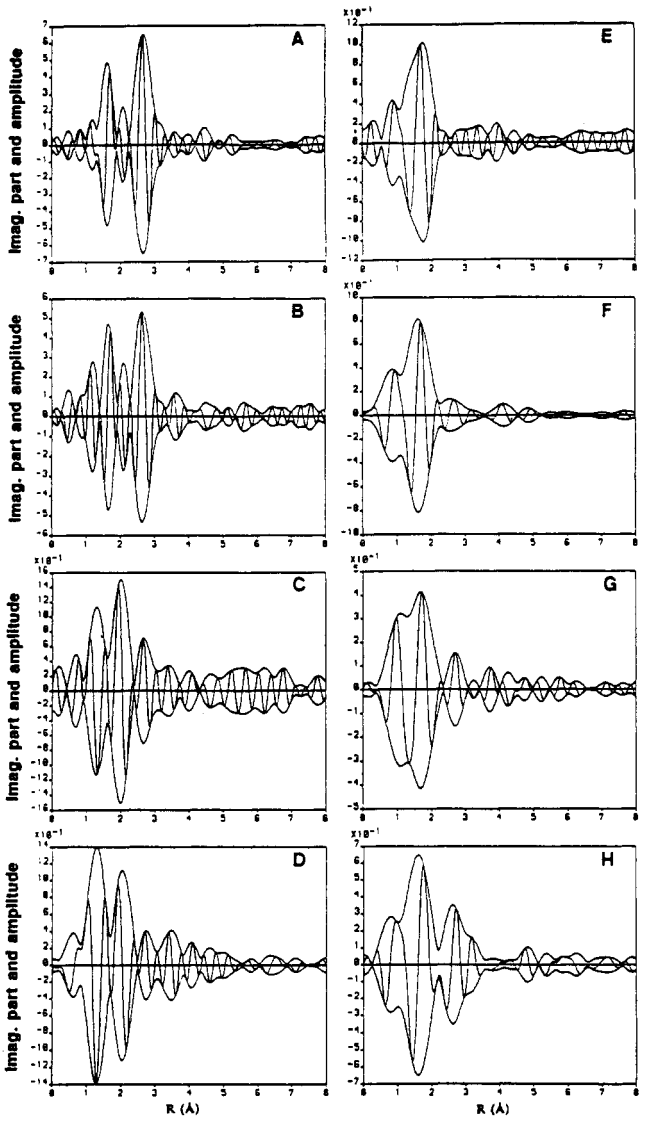

Figure 14. Fourier transformations of EXAFS samples, $Cl_2(THF)GeW(CO)_5$ in H6–Y. W edge spectra: (A) FT = k^3, 2.6–12 Å^{-1}, at room temperature; (B) FT = k^3, 2.6–12 Å^{-1}, at 120 °C; (C) FT = k^3, 2.6–12 Å^{-1}, at 150 °C; (D) FT = k^3, 2.6–12 Å^{-1}, at 250 °C. Ge edge spectra: (E) FT = k^2, 2.7–9 Å^{-1}, at room temperature; (F) FT = k^2, 2.7–9 Å^{-1}, at 120 °C; (G) FT = k^2, 2.7–9 Å^{-1}, at 150 °C; (H) FT = k^2, 2.7–9 Å^{-1}, at 250 °C.

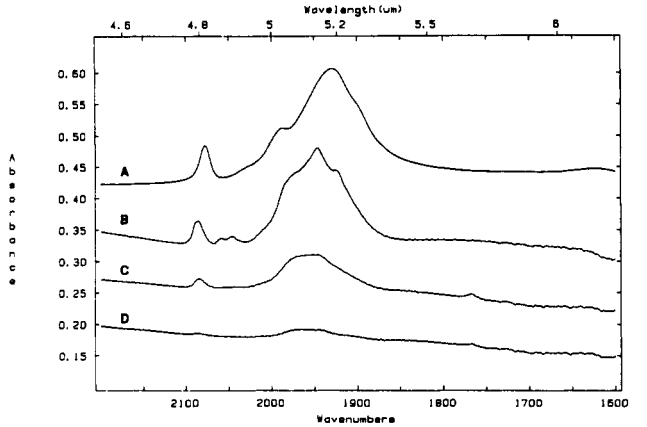

Figure 15. In situ FTIR spectra of $Cl_2(THF)GeW(CO)_5$: (A) in KBr, (B) in H6–Y at room temperature, (C) in H6–Y at 130 °C, (D) in H6–Y at 150 °C.

pure precursors, which have melting points of 86 and 106 °C, respectively, with concomitant decomposition.

A summary of the chemistry of precursor $Cl_2(THF)GeMo(CO)_5$ in zeolite cages of Na–Y and H6–Y is given in Scheme

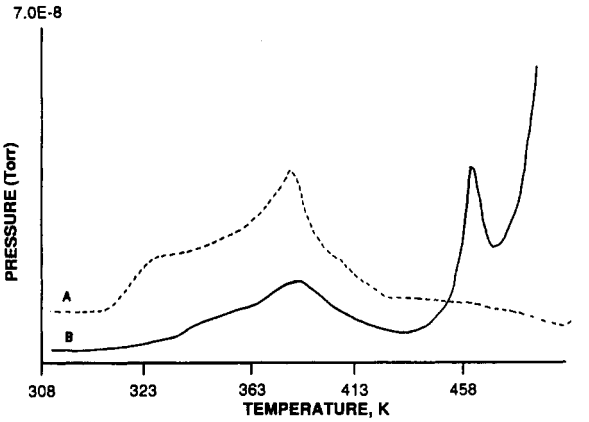

Figure 16. TPD-MS profiles of $Cl_2(THF)GeW(CO)_5$ in H6–Y, measured simultaneously with the FTIR spectra in Figure 15: (A) CO (mass 28); (B) HCl (mass 36), enlarged 10×.

SCHEME I: Anchoring and Thermal Decomposition of $Cl_2(THF)GeMo(CO)_5$ in Na–Y (Left) and H6–Y (Right) (Simplified)

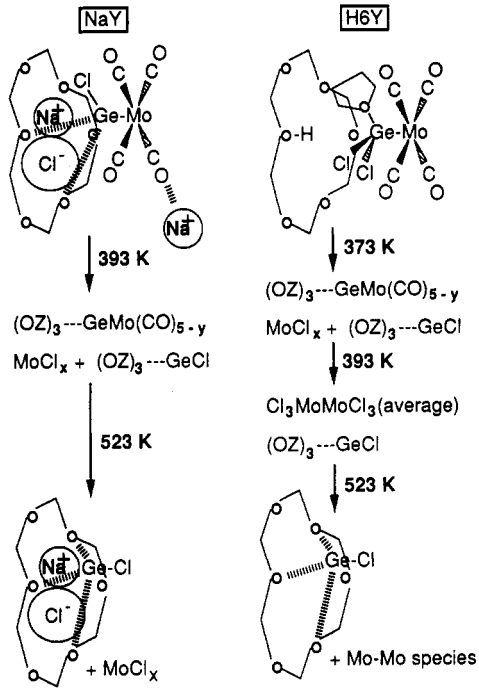

I. Slight decarbonylation occurs at room temperature in Na–Y and H6–Y. The complexes are somewhat more stable in Na–Y where complete loss of CO and transformation into molybdenum chloride species occurs between 120 and 250 °C. In H6–Y, this process is observed already at about 100 °C. Anchoring of the bimetallic complex occurs at room temperature in Na–Y, while in H6–Y attachment increases with temperature. Newly formed $MoCl_x$ species remain present in Na–Y until 250 °C, while they transform predominantly into Mo–Mo species in H6–Y.

In contrast to the molybdenum analog, no decarbonylation is detected for $Cl_2(THF)GeW(CO)_5$ in zeolites Na–Y and H6–Y up to about 100 °C (see Scheme II). The pentacarbonyl fragment then starts to transform into tungsten chloride compounds in Na–Y, which are stable at 250 °C. From the germanium edge data it is concluded that attachment to the framework occurs already at room temperature as for $Cl_2(THF)GeMo(CO)_5$ in Na–Y. This could be due to a strong Na^+--Cl^- interaction between the sodium ions in six-ring coordination sites and the chloride ligands of the precursor. Another interaction of sodium with the carbonyl complex in the form of Na^+--OC–M accounts for the complex IR pattern. Most importantly, we conclude that the range where the complex is intact *and* attached to the framework ranges from 25 to at least 100 °C in Na–Y. In H6–Y the majority of the complexes is still intact at 120 °C. Anchoring to the

SCHEME II: Anchoring and Thermal Decomposition of $Cl_2(THF)GeW(CO)_5$ in Na–Y (Left) and H6–Y (Right) (Simplified); Note: Intact Complex Anchored to H6–Y Zeolite at 100 °C)

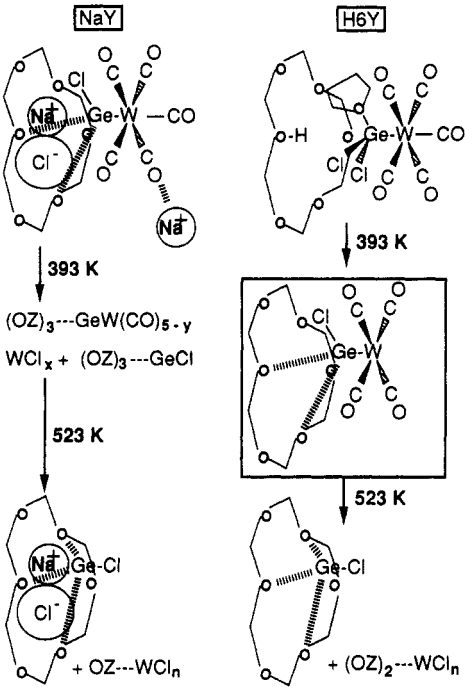

framework, however, increases only gradually with temperature.

These results show that carefully chosen bimetallic complexes can be anchored into cage systems of zeolites under retention of the Ge–metal bonds. The anchoring can prevent potential agglomeration under catalytic reaction conditions. The chemical reactivity of these anchored species is currently under investigation, and preliminary studies indicate ligand substitution at the transition-metal center.

Acknowledgment. We thank Professor D. C. Koningsberger for EXAFS software. Acknowledgment is made to the donors of the Petroleum Research Fund, administered by the American Chemical Society, and to the U.S. Department of Energy (Grant DE-FG04-90ER14158) for partial funding of this work. K.M. appreciates support from Sandia National Laboratories (DOE). The operational funds for NSLS beam line X-11A are supported by DOE Grant DE-AS0580ER10742.

References and Notes

(1) Lamb, H. H.; Gates, B. C.; Knözinger, H. *Angew. Chem., Int. Ed. Engl.* **1988**, *27*, 1127.
(2) Basset, J. M.; Choplin, A. *J. Mol. Catal.* **1983**, *21*, 95.
(3) Bailey, D. C.; Langer, S. H. *Chem. Rev.* **1981**, *81*, 109.
(4) Jardin, F. H. *Prog. Inorg. Chem.* **1981**, *28*, 63.
(5) Breck, D. W. *Zeolite Molecular Sieves*; Krieger: Malabar, FL, 1984.
(6) *New Developments in Zeolite Science and Technology*; Murakami, Y., Iijima, A., Ward, J. W., Eds.; Kodansha: Tokyo, 1986.
(7) Jacobs, P. A. *Carboniogenic Activity of Zeolites*; Elsevier: Amsterdam, 1977.
(8) Vervecken, M.; Servotte, Y.; Wydoodt, M.; Jacobs, L.; Martens, J. A.; Jacobs, P. A. In *Chemical Reactions in Organic and Inorganic Constrained Systems*; Setton, R., Ed.; Reidel: 1986, pp 95–114.
(9) Ballivet-Tkatchenko, D.; Coudurier, G.; Mozzanega, H.; Tkatchenko, I.; Kinnemann, A. *J. Mol. Catal.* **1979**, *6*, 293.
(10) Suib, S. L.; Kostapapas, A.; McMahon, K. C.; Baxter, J. C.; Winiecki, A. M. *Inorg. Chem.* **1985**, *24*, 858.
(11) Bein, T.; McLain, S. J.; Corbin, D. R.; Farlee, R. F.; Moller, K.; Stucky, G. D.; Woolery, G.; Sayers, D. *J. Am. Chem. Soc.* **1988**, *110*, 1801.
(12) Herron, N.; Stucky, G. D.; Tolman, C. A. *Inorg. Chim. Acta* **1985**, *100*, 135.
(13) Bein, T.; Schmiester, G.; Jacobs, P. A. *J. Phys. Chem.* **1986**, *90*, 4851.
(14) Yang, Y. S.; Howe, R. F. In *New Developments in Zeolite Science and Technology*; Murakami, Y.; Iijima, A.; Ward, J. W., Eds.; Kodansha: Tokyo, 1986; p 883.
(15) Verdonck, J. J.; Schoonheydt, R. A.; Jacobs, P. A. *J. Phys. Chem.* **1983**, *87*, 683.
(16) Gelin, P.; Naccache, C.; Ben Taarit, Y.; Diab, Y. *Nouv. J. Chim.* **1984**, *8*, 675.
(17) Bergeret, G.; Gallezot, P.; Gelin, P.; Ben Taarit, Y.; Lefebvre, F.; Naccache, C.; Shannon, R. D. *J. Catal.* **1987**, *104*, 279.
(18) Davis, M. E.; Schnitzer, J.; Rossin, J. A.; Taylor, D.; Hanson, B. E. *J. Mol. Catal.* **1987**, *39*, 243.
(19) Shannon, R. D.; Vedrine, J. C.; Nacchache, C.; Lefebvre, F. *J. Catal.* **1984**, *88*, 431.
(20) Diegruber, H.; Plath, P. J.; Schulz-Ekloff, G. *J. Mol. Catal.* **1984**, *24*, 115.
(21) Herron, N.; Stucky, G. D.; Tolman, C. A. *J. Chem. Soc., Chem. Commun.* **1986**, 1521.
(22) Yermakov, Yu. I. *Catal. Rev.—Sci. Eng.* **1976**, *13*, 77.
(23) Foley, H. C.; DeCanio, S. J.; Tau, K. D.; Chao, K. J.; Onuferko, J. H.; Dybowski, C.; Gates, B. C. *J. Am. Chem. Soc.* **1983**, *105*, 3074.
(24) Ward, M. D.; Schwartz, J. *J. Mol. Catal.* **1981**, *11*, 397.
(25) Huang, T. N.; Schwartz, J.; Kitajima, N. *J. Mol. Catal.* **1984**, *22*, 389.
(26) Huang, T. N.; Schwartz, J. *J. Am. Chem. Soc.* **1982**, *104*, 5244.
(27) Corbin, D. R.; Seidel, W. C.; Abrams, L.; Herron, N.; Stucky, G. D.; Tolman, C. A. *Inorg. Chem.* **1985**, *24*, 1800.
(28) Taylor, D. F.; Hanson, B. E.; Davis, M. E. *Inorg. Chim. Acta* **1987**, *128*, 55.
(29) Borvornwattananont, A.; Moller, K.; Bein, T. *J. Chem. Soc., Chem. Commun.* **1990**, 28.
(30) Behrens, H.; Moll, M.; Sixtus, E. *Z. Naturforsch.* **1977**, *32b*, 1105.
(31) Grim, S. O. *J. Am. Chem. Soc.* **1967**, *89*, 5573.
(32) Minelli, M.; Maley, W. J. *Inorg. Chem.* **1989**, *28*, 2954.
(33) Braterman, P. S.; Milne, D. W.; Randall, E. W.; Rosenberg, E. *J. Chem. Soc., Dalton Trans.* **1973**, 1027.
(34) Lee, P. A.; Citrin, P. H.; Eisenberger, P.; Kincaid, B. M. *Rev. Mod. Phys.* **1981**, *53*, 769.
(35) Du Mont, W.-W.; Lange, L.; Pohl, S.; Saak, W. *Organometallics* **1990**, *9*, 1395.
(36) Petz, W. *Chem. Rev.* **1986**, *86*, 1019.
(37) Applying a k^3-weighting factor for the Fourier transformation, these three shells are more resolved and fitting was carried out with this spectrum. The fit results show that there is still some carbonyl coordination (0.6 carbon atoms at a distance of 2.08 Å and 1.0 oxygen atoms at a distance of 3.14 Å). Using a narrow back-transform range between 1.7 and 2.2 Å for the middle shell, the inverse FT spectrum compared more to that of the Mo–Cl reference than to Mo–Ge. The final fitting procedure was performed over a wider range of 1.3–2.2 Å with both carbon and Mo–Cl or $MoSe_2$ as reference for a possible Mo–Ge contribution. A good fit result was obtained with a coordination of 1.4 Cl atoms at a distance of 2.53 Å. Only one dominant peak remains upon heating the sample in Na–Y up to 250 °C (Figure 6C) at which all carbonyls vanished (this is supported by IR data of the same sample). This peak resembles the middle peak in sample GeMo(Na12). Using k^3-weighted FT, the spectrum (not shown) reveals an additional shoulder at the right side of the main peak. After isolating this shoulder by an appropriate back-transformation the spectrum of the main peak could be fitted with the Mo–Cl reference.
(38) It should be noted that the temperatures of the in situ experiments may not be compared directly to the temperatures of the EXAFS batch experiments due to different sample amounts and geometries, with different resulting partial pressures at the zeolite crystal surfaces.
(39) Cotton, F. A.; Wilkinson, G. *Advanced Inorganic Chemistry*; 5th ed.; Wiley: New York, 1988, p 840.